


Article

# Optimization of Connection Parameters of Self-Adaptive Modular Floating Wind Farms

Yuming Zhang <sup>1</sup>, Da Li <sup>1</sup> and Haixiao Liu <sup>2,\*</sup> 

<sup>1</sup> CNOOC Research Institute Ltd., Beijing 100028, China; zhangym72@cnooc.com.cn (Y.Z.)

<sup>2</sup> School of Civil Engineering, Tianjin University, Tianjin 300072, China

\* Correspondence: liuhx@tju.edu.cn

**Abstract:** Connection parameters are the key factors influencing the responses of modular floating structures; due to the complexity of structural response properties, the assessment and optimization of connection parameters are still vital issues in designing modular floating structures. In the present work, for a novel structural configuration of self-adaptive modular floating wind farms based on existing works from the case of a mobile offshore base, a quantified approach for the assessment of connection parameters is established based on frequency domain numerical analysis taking into account both the economic effects and generalized performance. Based on the quantified assessment, an optimization process is carried out, to obtain a connection parameter combination. From the optimized connection parameters, it can be found that the most appropriate tri-axial stiffness according to present studies is in the magnitude from  $1 \times 10^6$  to  $7 \times 10^7$  N/m, and the damping ratio is close to 1.0 for most connection structures. By contrast with feasible uniform connection parameters, the optimization methodology is confirmed to be able to reduce both connection parameters and responses. Then, a time domain approach for the calculation of motions of interconnected modular floating structures taking into account geometry nonlinearity is proposed and obtained in good accordance with the frequency domain results, and the effectiveness of both the frequency domain and time domain is validated.

**Keywords:** modular floating structure; connection parameter; optimization; floating wind turbine; time domain analysis; hydroelasticity



**Citation:** Zhang, Y.; Li, D.; Liu, H. Optimization of Connection Parameters of Self-Adaptive Modular Floating Wind Farms. *J. Mar. Sci. Eng.* **2024**, *12*, 1840. <https://doi.org/10.3390/jmse12101840>

Academic Editor: Bang-Fuh Chen

Received: 29 July 2024

Revised: 28 September 2024

Accepted: 8 October 2024

Published: 14 October 2024



**Copyright:** © 2024 by the authors. Licensee MDPI, Basel, Switzerland. This article is an open access article distributed under the terms and conditions of the Creative Commons Attribution (CC BY) license (<https://creativecommons.org/licenses/by/4.0/>).

## 1. Introduction

With offshore wind going to deeper waters in recent years, due to their feasibility in deepwater environments, floating wind turbines have gained popularity. Compared with fixed wind turbines, floating wind turbines are in the early stage of application, with cost being the major concern. NREL carried out research on the costs of wind turbines indicating the cost of floating wind turbines to be 1.5 times that of fixed offshore wind turbines and 3 times that of land-based ones [1]. If the costs remain unchanged the commercialization of floating wind turbines would not be possible.

At present, the structural configurations of floating wind turbines are mainly from oil and gas platforms, in the form of semisubmersibles, spars, and TLPs [2], and one turbine for each floating foundation. Besides the traditional types, concepts for new structural configurations have been proposed in which two turbines are located on one floating foundation, for this type of FOWT, single-point positioning is usually adopted as the method for heading adjustment of the turbines rather than yaw control systems due to weather-vane effects [3,4]. Early in 2008, Manabe H et al. proposed the concept of self-sailing floating wind farms, in which multiple wind turbines are installed on one floating foundation integrated with the sailing, hydrogen-making abilities [5].

To reduce the costs of floating wind turbines, in our previous work [6], a new type of floating wind farm was proposed by integrating floating wind turbines with single-point

positioning and modular floating structures (Figure 1). This new type of floating wind farm is self-adaptive to wind direction, i.e., has the ability to adjust its heading to wind inflow, avoiding the shadowing effects between wind turbines. As all wind turbines are installed on one floating foundation, the new structure type has great potential for integration, such as with photovoltaics; meanwhile, the inter-turbine cables will be placed on board, saving the costs of array cable installation and maintenance. The self-adaptive floating wind farm is large in space occupation and can be categorized as a very large floating structure [7]. Due to its large size, the wind farm is composed of multiple inter-connected floating modules, i.e., it is a modular floating structure.

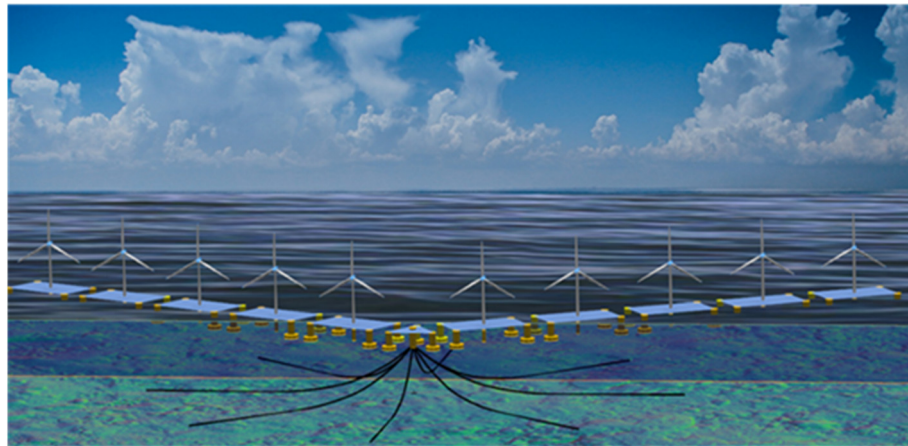


**Figure 1.** Concept of the modular self-adaptive wind farm.

Different from single-body floating structures, modular floating structures are usually composed of multiple inter-connected floating modules. Due to the special structural configuration, the wave loads on different modules vary in amplitudes and phases, and the motions of the modules will cause an additional hydrodynamic load (radiation effects); meanwhile, the motions of modules will induce connection loads imposed on adjacent modules via connection structures, i.e., both hydrodynamic coupling and structural coupling exist in the hydroelastic properties of modular floating structures [8,9].

The concept of modular floating structures is widely adopted in floating breakwaters, floating wave energy converters, and very large floating structures. Since the 1990s extensive work has been carried out on the numerical approaches for the analysis of dynamic responses to modular floating structures in the form of mobile offshore bases [10,11], floating wave energy converters [12,13], floating breakwaters [14], etc. Based on the knowledge obtained from the mobile offshore base, for modules whose elasticity is not significant, like semisubmersible modules, the rigid-module-elastic-connection model (RMFC) is adequate in the analysis of dynamic responses [15,16].

On account of the structural coupling effects, the connection parameters play a vital role in the dynamic responses of modular floating structures. Due to the variety in functions and structural configurations, the requirements for the connection parameters vary with structural configuration. Unlike the issues in the approach of the numerical analysis method, research on the assessment and optimization of connection parameters is not as abundant. Zhang et.al [17] proposed a generalized method to assess the connection parameters taking into account both economic effects and general performances of the structures and applied it to the optimization of connection parameters for a modular floating wave energy converter and a mobile offshore base in the preliminary design phase.

For the modular floating wind farm in the present work, existing work mainly focuses on the self-adaptive properties and wake properties [18,19]. Few works have been carried out on the hydroelastic properties. Meanwhile, for a modular floating structure with a weather-vane ability, the geometric nonlinearity in the connection structures will lead to inaccuracy in the calculation of connection loads. In the present work, following the example

of existing work on the mobile offshore base, a quantified method to assess the connection parameters of a modular floating wind farm is proposed, and the process of optimization is carried out taking into account both economic effects and general performance based on frequency domain analysis. Then, a methodology for the calculation of connection loads in the time domain is proposed, and good accordance is obtained between frequency domain results and time domain results.

### 2. Data of the Floating Structure

The modular floating farm is composed of six wind turbine modules (marked T1–T6 henceforth), and a center-of-yawing module (marked COY henceforth), as shown in Figure 2. Due to the high requirements on the out-of-horizontal-plane motions of the modules induced by the wind turbines, four connection structures are arranged for adjacent modules as single-point connections. In the present work, connection structures are simplified as combinations of tri-axial stiffness and damping, which resemble the viscous dampers; when there is no environmental load, the connection structures stay undeformed, and the locations of connection points calculated from adjacent modules will be identical. When relative motions between adjacent modules occur, deviations in the locations of connection points will be calculated from different modules, which will be taken as the deformation of the connection structures; similarly the ratio of deformation can be obtained by replacing the deviation of location with the relative velocity. When the deformation and its rate are obtained, the viscoelasticity of the connection structure can be calculated. To obtain the global optimum, anisotropic connection parameters are adopted, i.e., tri-axial stiffness and tri-axial damping ratios for each connection parameter, six connection parameters for each connection structure. Due to the symmetry of the modules, in the optimum solution, connection parameters symmetric to the COY module will be equal (like C1 and C7, C4 and C10); therefore, the number of connection parameters for optimization is 72. The water depth is 200 m, the mooring line from the OC4 semi-submersible wind turbine [20] is adopted, the fairlead for single-point mooring is (0, 0, −20 m), and eight spread mooring lines with a uniform gap of 45° in between are adopted (Figure 2).

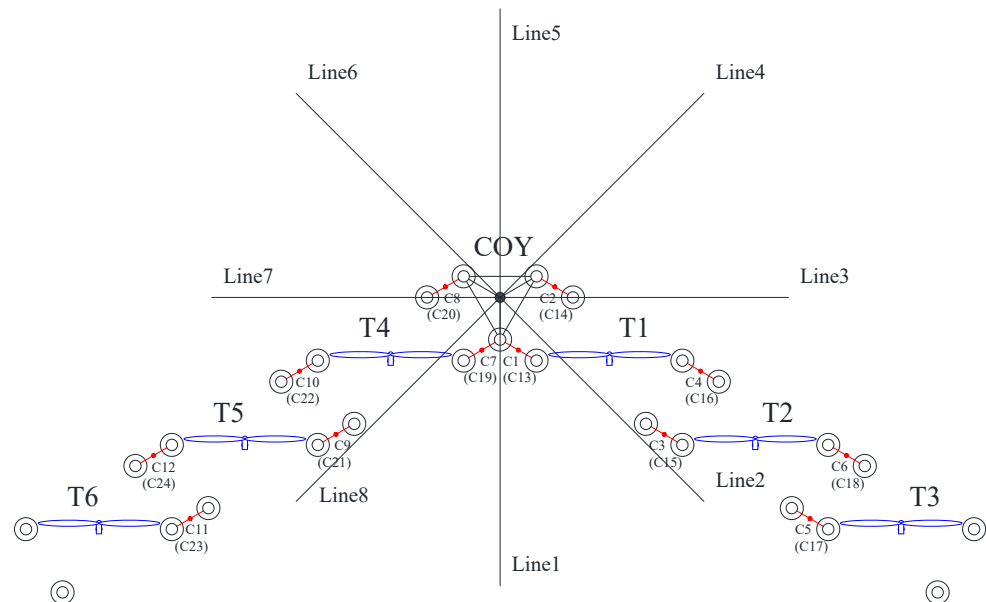


**Figure 2.** Layout and numbering of modules, connection structures (in red), and mooring lines.

For the convenience of structural design, the connection point is set to the center point between adjacent pontoons and the upper connection structures are 8 m above the waterline, while the lower ones are 17 m below the waterline. The numbering of connection structures is shown in Figure 2, the ones in brackets are lower connection structures. The sizes and

weights of the pontoons are the same as the ones from the NREL OC4 semisubmersible floating foundation and the NREL 5WM wind turbine is selected [21]. Geometric features, dimensions, spacings of modules, and the simplification of connection structures are shown in Figure 3; the dynamic features of the wind turbine modules and COY modules are shown in Table 1, and the coordinates of connection points relative to COGs of modules are shown in Table 2 (take the example of the COY module and T1, the rest can be easily inferred).

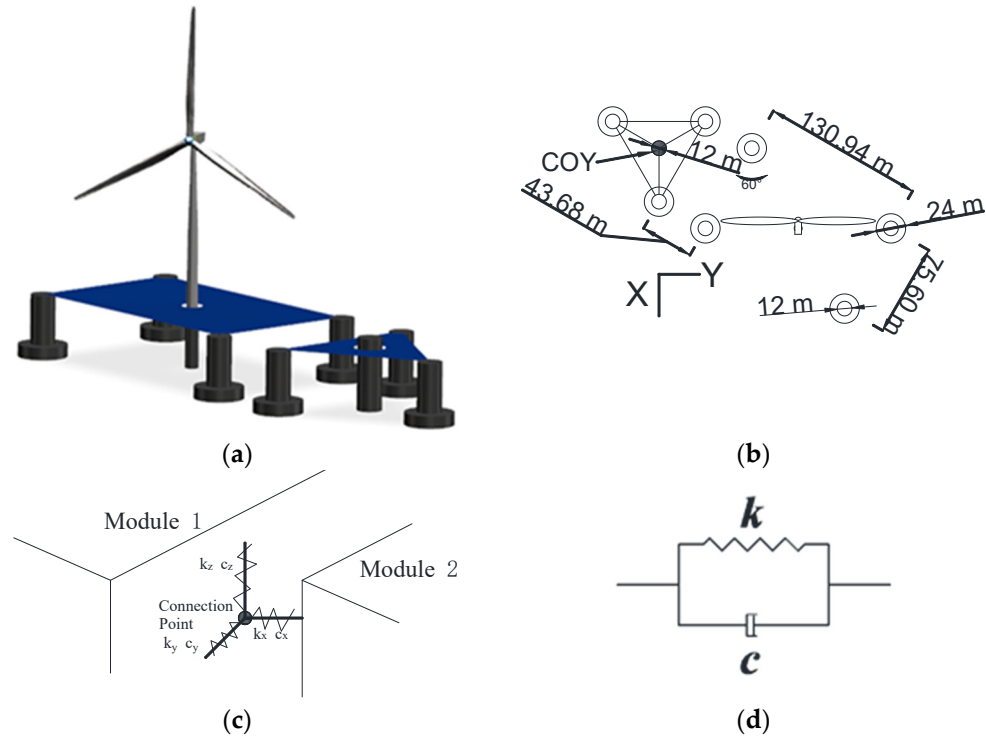


**Figure 3.** Geometry, key dimensions of the modules, simplification, and mechanical model of connection structures: (a) 3D geometry; (b) key dimensions; (c) connection structure simplification; (d) mechanical model.

**Table 1.** Parameters of the modules.

	Unit	COY Module	Turbine Module
Mass	kg	$1.322 \times 10^7$	$1.83 \times 10^7$
$I_{xx}$	$\text{kgm}^2$	$1.22 \times 10^{10}$	$6.651 \times 10^{10}$
$I_{yy}$	$\text{kgm}^2$	$1.22 \times 10^{10}$	$4.161 \times 10^{10}$
$I_{zz}$	$\text{kgm}^2$	$2.37 \times 10^{10}$	$9.958 \times 10^{10}$
Draft	m	20	20
KG (COG to keel)	m	5.75	8.26

**Table 2.** Coordinates of the connection structures relative to the COGs.

Connection	COY	T1
C1	(54.56, 18.9, 22.25)	(−10.91, −94.5, 19.74)
C2	(−10.91, 56.7, 22.25)	(−76.38, −56.7, 19.74)
C13	(54.56, 18.9, −2.75)	(−10.91, −94.5, −5.26)
C14	(−10.91, 56.7, −2.75)	(−76.38, −56.7, −5.26)
C3	-	(76.38, 56.7, 19.74)
C4	-	(10.91, 94.5, 19.74)
C15	-	(76.38, 56.7, −5.26)
C16	-	(10.91, 94.5, −5.26)



### 3. Methodology for the Optimization of Connection Parameters

#### 3.1. Frequency Domain Analysis Method

For interconnected multi-body floating structures without a mooring system, the frequency domain dynamic equation is:

$$F_c = -A_c^T((K_c - i\omega C_c)A_c)u \tag{1}$$

where  $\omega$  is the wave frequency;  $M$  denotes the matrix of mass and is a diagonal matrix with the size of  $42 \times 42$ ;  $A$  and  $B$  are the matrices of first-order hydrodynamic added mass and damping, obtained from hydrodynamic analysis [22];  $C$  is the matrix of hydrostatic stiffness;  $u$  denotes the 6-DOF responses of the module COGs under wave amplitude of 1 m and is the solution of the equation;  $F_w$  is the 42-component complex vector of wave excitation loads, obtained from hydrodynamic analysis; and  $F_c$  is the 42-component complex vector of connection loads on the COGs of the modules, calculated from:

$$F_c = -A_c^T((K_c - i\omega C_c)A_c)u \tag{2}$$

where,  $A_c$  is the matrix of connection, composed of the relative coordinates between connection points and the COGs of the modules [23];  $K_c$  is the matrix of connection stiffness in the form of a diagonal matrix, with its components as the tri-axial stiffness of connection structures; and  $C_c$  is the matrix of damping, also a diagonal matrix in a form similar to  $K_c$ . In the present work, the damping of the connection structures is presented in the form of a damping ratio which is as follows:

$$c_i = 2\eta_i\sqrt{mk_i} \tag{3}$$

where  $c_i$  is the actual damping,  $\eta_i$  is the damping ratio,  $m$  is the mass of the wind turbine modules, and  $k_i$  is the stiffness of the connection structure.

When the responses of the COGs of modules are obtained, the responses of the hubs of the wind turbines can be obtained as:

$$u_{HUB} = A_{HUB}u_{COG} \tag{4}$$

where  $A_{HUB}$  is the matrix of conversion from COG to hub and can be obtained from rigid body kinematics.

Connection loads  $F_{cc}$  can be calculated as:

$$F_{cc} = ((K_c - i\omega C_c)A_c)u \tag{5}$$

Under irregular waves, the significant responses  $R_{isign}$  can be calculated as:

$$R_{isign} = 2\sqrt{m_0}, m_0 = \int_0^{+\infty} u_i^2(\omega)S(\omega)d\omega \tag{6}$$

where  $S(\omega)$  is the spectral density of the irregular wave.

The extreme value for responses can be calculated as:

$$R_{iex} = 1.86R_{isign} \tag{7}$$

Response amplitude under irregular waves  $X_{spec}(\omega)$  can be calculated as:

$$X_{spec}(\omega) = \sqrt{u_i^2(\omega)S(\omega)\Delta\omega} \tag{8}$$

where  $\Delta\omega$  is the interval between wave components in the process of discretization of irregular waves.

### 3.2. Time Domain Analysis Method

To obtain connection loads in the time domain, a methodology for the calculation of time domain connection loads fully taking into account the geometry nonlinearity of connection structures is proposed.

Due to rigid module assumption, the position of connection points  $(x_{con}, y_{con}, z_{con})$  can be obtained from the motions of the modules based on rigid body kinematics:

$$\begin{bmatrix} x_{con} \\ y_{con} \\ z_{con} \end{bmatrix} = \begin{bmatrix} x_g \\ y_g \\ z_g \end{bmatrix} + \begin{bmatrix} \cos\theta_2\cos\theta_3 & \sin\theta_1\sin\theta_2\cos\theta_3 - \cos\theta_1\sin\theta_3 & \cos\theta_1\sin\theta_2\cos\theta_3 + \sin\theta_1\sin\theta_3 \\ \cos\theta_2\sin\theta_3 & \sin\theta_1\sin\theta_2\sin\theta_3 + \cos\theta_1\cos\theta_3 & \cos\theta_1\sin\theta_2\sin\theta_3 - \sin\theta_1\cos\theta_3 \\ -\sin\theta_2 & \sin\theta_1\cos\theta_2 & \cos\theta_1\cos\theta_2 \end{bmatrix} \begin{bmatrix} x_{con-g} \\ y_{con-g} \\ z_{con-g} \end{bmatrix} \quad (9)$$

where,  $[x_g \ y_g \ z_g]^T$  is the coordinate of the COG,  $[x_{con-g} \ y_{con-g} \ z_{con-g}]^T$  is the coordinate of the connection point in the local coordinate system of the module centered with its COG, and  $[\theta_1 \ \theta_2 \ \theta_3]^T$  is the instantaneous rotational response of the module.

When the position of the connection is obtained, the velocity of the connection point  $[v_{con-x} \ v_{con-y} \ v_{con-z}]^T$  can be calculated as:

$$\begin{bmatrix} v_{con-x} \\ v_{con-y} \\ v_{con-z} \end{bmatrix} = \begin{bmatrix} v_{g-x} \\ v_{g-y} \\ v_{g-z} \end{bmatrix} + \begin{bmatrix} 0 & z_{con} - z_g & -(y_{con} - y_g) \\ -(z_{con} - z_g) & 0 & x_{con} - x_g \\ y_{con} - y_g & -(x_{con} - x_g) & 0 \end{bmatrix} \begin{bmatrix} \dot{\theta}_1 \\ \dot{\theta}_2 \\ \dot{\theta}_3 \end{bmatrix} \quad (10)$$

where  $[v_{g-x} \ v_{g-y} \ v_{g-z}]^T$  is the velocity of the COG of the module, and  $[\dot{\theta}_1 \ \dot{\theta}_2 \ \dot{\theta}_3]^T$  is the rotational velocity of the module.

When the positions and velocities of the connection points are obtained, the deformation and deformation rate of connection structures can be obtained from the difference in connection point position and the velocities calculated from adjacent modules, i.e.,  $[\Delta x_{con} \ \Delta y_{con} \ \Delta z_{con}]^T$  is the deformation of the connection structure, and  $[\Delta v_{con-x} \ \Delta v_{con-y} \ \Delta v_{con-z}]^T$  is the deformation rate of the connection structure, both the deformation and its rate are in the global coordinate system.

For a modular floating structure with weather-vane ability, a large yaw response will induce great variations in the global connection stiffness, for instance, a 90° yaw response will lead to an exchange in  $k_x$  and  $k_y$ . Therefore, the calculation of connection loads should be based on the deformations in the local coordinates of the modules, i.e., coordinate conversion from the global coordinate system to the local coordinate system is required.

Conversion to the local coordinate system can be applied with the inverse of the Euler angle conversion matrix:

$$\begin{bmatrix} \Delta x_{con-g} \\ \Delta y_{con-g} \\ \Delta z_{con-g} \end{bmatrix} = \begin{bmatrix} \cos\theta_2\cos\theta_3 & \sin\theta_1\sin\theta_2\cos\theta_3 - \cos\theta_1\sin\theta_3 & \cos\theta_1\sin\theta_2\cos\theta_3 + \sin\theta_1\sin\theta_3 \\ \cos\theta_2\sin\theta_3 & \sin\theta_1\sin\theta_2\sin\theta_3 + \cos\theta_1\cos\theta_3 & \cos\theta_1\sin\theta_2\sin\theta_3 - \sin\theta_1\cos\theta_3 \\ -\sin\theta_2 & \sin\theta_1\cos\theta_2 & \cos\theta_1\cos\theta_2 \end{bmatrix}^{-1} \begin{bmatrix} \Delta x_{con} \\ \Delta y_{con} \\ \Delta z_{con} \end{bmatrix} \quad (11)$$

where  $[\Delta x_{con-g} \ \Delta y_{con-g} \ \Delta z_{con-g}]^T$  is the deformation of the connection structure under the local coordinate system; the deformation rate under the local coordinate system  $[\Delta v_{con-xg} \ \Delta v_{con-yg} \ \Delta v_{con-zg}]^T$  can be obtained with a similar method.

When the deformation and deformation rate under local coordinates are obtained, the connection force can be calculated as:

$$\begin{bmatrix} f_{c-xg} \\ f_{c-yg} \\ f_{c-zg} \end{bmatrix} = - \begin{bmatrix} k_{cx} & 0 & 0 \\ 0 & k_{cy} & 0 \\ 0 & 0 & k_{cz} \end{bmatrix} \begin{bmatrix} \Delta x_{con-g} \\ \Delta y_{con-g} \\ \Delta z_{con-g} \end{bmatrix} - \begin{bmatrix} c_{cx} & 0 & 0 \\ 0 & c_{cy} & 0 \\ 0 & 0 & c_{cz} \end{bmatrix} \begin{bmatrix} \Delta v_{con-xg} \\ \Delta v_{con-yg} \\ \Delta v_{con-zg} \end{bmatrix} \quad (12)$$

where,  $[f_{c-xg} \ f_{c-yg} \ f_{c-zg}]^T$  is the tri-axial loading under the local coordinate system and is the export of connection loads.

As the equation of the dynamic response is in the global coordinate system, the connection loads need to be converted into the global coordinate system, as follows:

$$\begin{bmatrix} f_{c-x} \\ f_{c-y} \\ f_{c-z} \end{bmatrix} = \begin{bmatrix} \cos\theta_2\cos\theta_3 & \sin\theta_1\sin\theta_2\cos\theta_3 - \cos\theta_1\sin\theta_3 & \cos\theta_1\sin\theta_2\cos\theta_3 + \sin\theta_1\sin\theta_3 \\ \cos\theta_2\sin\theta_3 & \sin\theta_1\sin\theta_2\sin\theta_3 + \cos\theta_1\cos\theta_3 & \cos\theta_1\sin\theta_2\sin\theta_3 - \sin\theta_1\cos\theta_3 \\ -\sin\theta_2 & \sin\theta_1\cos\theta_2 & \cos\theta_1\cos\theta_2 \end{bmatrix} \begin{bmatrix} f_{c-xg} \\ f_{c-yg} \\ f_{c-zg} \end{bmatrix} \quad (13)$$

When the connection loads are obtained, the time domain responses can be calculated through the dynamic equation of:

$$(M + A_\infty)\ddot{X}(t) + B\dot{X}(t) + CX(t) + \int_0^t h(t - \tau)\ddot{X}(\tau)d\tau = F_w(t) + \sum T_i(t) + F_C \quad (14)$$

where,  $A_\infty$  is the added mass at infinite frequency;  $F_w$  is the time domain wave loads;  $T_i$  is the loads from the mooring system on the modules;  $F_c$  is the vector of connection loads, whose components can be calculated from Equation (9) to Equation (13); and  $h(t)$  is the matrix of impulse function, defined as:

$$h(t) = \frac{2}{\pi} \int_0^\infty (A(\omega) - A_\infty)\cos(\omega t)d\omega \quad (15)$$

### 3.3. Constraints for Optimization

For the modular floating wind farm, in the present work, two working conditions are taken as the basis for optimization, the operation condition and the survival condition. In the operation condition, wind turbines are running, and constraints on the motions of the modules are made based on the constraints of the wind turbine operation; meanwhile, for the survival condition, the operation of wind turbines is ceased, and the constraints on the module responses are made on the survival limits of the floating foundations and wind turbines.

In the present work, generalized wave conditions are adopted as working conditions, the Sea State 6 (SS6  $H_s = 5$  m,  $T_p = 12.4$  s, 15.03% percentage of probability in Northern Pacific ) and Sea State 7 (SS7  $H_s = 7.5$  m,  $T_p = 15$  s, 7% percentage of probability in Northern Pacific) waves [24] are taken as the operational condition and survival condition; spectral density for the two conditions are shown in Figure 4, due to the self-adaptive property of the floating structure, heading waves are taken as the only environment condition for optimization. When the location of deployment is specified, the optimization will be based on real environmental parameters and distributions.

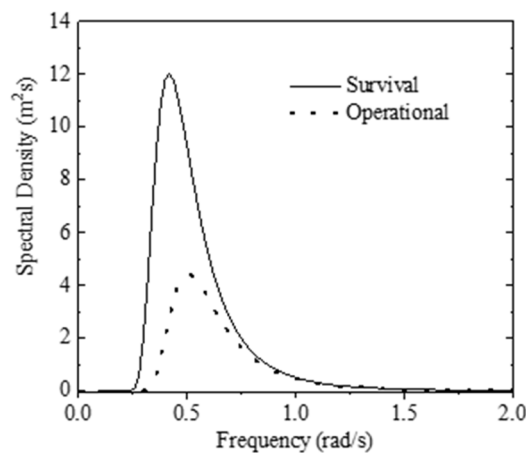


Figure 4. Spectral densities for survival and operational conditions.

In the present work, due to the lack of specified turbine data, the constraints on the modules are assumed as shown in Table 3, when real turbine data are acquired, the constraints would be altered.

**Table 3.** Constraints on the responses of the structures.

Type	DOF	Unit	Point	Condition	Response	Value
Motion	Roll	°	COG	Survival	Extreme	10
Motion	Pitch	°	COG	Survival	Extreme	8
Motion	Heave	m	COG	Operational	Extreme	4
Motion	Roll	°	COG	Operational	Significant	3
Motion	Pitch	°	COG	Operational	Significant	3
Motion	Yaw	°	COG	Operational	Significant	1.5
Velocity	Surge	m/s	HUB	Operational	Significant	1
Velocity	Sway	m/s	HUB	Operational	Significant	1
Acceleration	Surge	g	HUB	Operational	Extreme	0.1
Acceleration	Sway	g	HUB	Operational	Extreme	0.1
Acceleration	Heave	g	HUB	Operational	Extreme	0.4

Based on frequency domain analysis, the constraints on the modules would be:  
Under survival conditions:

$$1.86 \times 2 \sqrt{\int_{\omega_{\min}}^{\omega_{\max}} S_S(\omega) \text{diag}(\text{vabs}(\mathbf{u}(\omega))) \text{vabs}(\mathbf{u}(\omega)) d\omega} \prec \mathbf{X}_S \tag{16}$$

Under operational conditions:

$$\left\{ \begin{array}{l} 2 \sqrt{\int_{\omega_{\min}}^{\omega_{\max}} S_O(\omega) \text{diag}(\text{vabs}(\mathbf{u}(\omega))) \text{vabs}(\mathbf{u}(\omega)) d\omega} \prec \mathbf{X}_O \\ 2 \sqrt{\int_{\omega_{\min}}^{\omega_{\max}} S_O(\omega) \text{diag}(\text{vabs}(\omega \mathbf{A}_{HUB} \mathbf{u}(\omega))) \text{vabs}(\omega \mathbf{A}_{HUB} \mathbf{u}(\omega)) d\omega} \prec \mathbf{V}_O \\ 1.86 \times 2 \sqrt{\int_{\omega_{\min}}^{\omega_{\max}} S_O(\omega) \text{diag}(\text{vabs}(\omega^2 \mathbf{A}_{HUB} \mathbf{u}(\omega))) \text{vabs}(\omega^2 \mathbf{A}_{HUB} \mathbf{u}(\omega)) d\omega} \prec \mathbf{a}_O \end{array} \right. \tag{17}$$

where  $S_s(\omega)$  denotes the wave spectral density of the survival condition;  $S_0(\omega)$  denotes the spectral density of the operation condition; “vabs” is a function to convert the input vector into a vector whose components are the absolute values of corresponding ones of the input; the symbol “ $\prec$ ” means that each component of the vector on the left is below the corresponding one on the right; the symbol of square root here is meant for calculating the square root of each component of the vector;  $\mathbf{u}(\omega)$  denotes the responses of the wind turbine modules; and  $\mathbf{X}_s$ ,  $\mathbf{X}_o$ ,  $\mathbf{V}_o$ , and  $\mathbf{a}_o$  are constraint vectors on the responses of the wind turbine modules, written as:

$$\left\{ \begin{array}{l} \mathbf{X}_S = (\mathbf{X}_{S-M}, \mathbf{X}_{S-M}, \mathbf{X}_{S-M}, \mathbf{X}_{S-M}, \mathbf{X}_{S-M}, \mathbf{X}_{S-M})^T \\ \mathbf{X}_O = (\mathbf{X}_{O-M}, \mathbf{X}_{O-M}, \mathbf{X}_{O-M}, \mathbf{X}_{O-M}, \mathbf{X}_{O-M}, \mathbf{X}_{O-M})^T \\ \mathbf{V}_O = (\mathbf{V}_M, \mathbf{V}_M, \mathbf{V}_M, \mathbf{V}_M, \mathbf{V}_M, \mathbf{V}_M)^T \\ \mathbf{a}_O = (\mathbf{a}_M, \mathbf{a}_M, \mathbf{a}_M, \mathbf{a}_M, \mathbf{a}_M, \mathbf{a}_M)^T \end{array} \right. \tag{18}$$

where,  $\mathbf{X}_{S-M}$ ,  $\mathbf{X}_{O-M}$ ,  $\mathbf{V}_M$ , and  $\mathbf{a}_M$  are the constraints on the motions, velocities, and accelerations of modules, defined as:

$$\left\{ \begin{array}{l} \mathbf{X}_{S-M} = (\infty, \infty, \infty, 10^\circ, 10^\circ, \infty) \\ \mathbf{X}_{O-M} = (\infty, \infty, 2.151\text{m}, 3^\circ, 3^\circ, 1.5^\circ) \\ \mathbf{V}_M = (1\text{m/s}, 1\text{m/s}, \infty, \infty, \infty, \infty) \\ \mathbf{a}_M = (0.1\text{g}, 0.1\text{g}, 0.4\text{g}, \infty, \infty, \infty) \end{array} \right. \tag{19}$$

The sign of infinity denotes the response is unconstrained.

### 3.4. Construction of the Target Function

As a complex multi-body system, the responses of the modular floating wind farm are complex, and the variations in dynamic responses with connection parameters would not be simple. For different types of dynamic responses, the optimization preference for

connection parameters may be contradictory; meanwhile, some types of dynamic responses are not quite sensitive to the variations in connection parameters. Due to the complexities stated above, the methodology to assess the connection parameters would take into account all factors.

In the present work, an integrated method is adopted to quantitatively assess the connection parameters.

The connection structures are given in the form of a serial and parallel arrangement of connection [17] (Figure 5). Therefore, the goal of optimization is to obtain the balance between the number of connection elements and the performances of the structure.

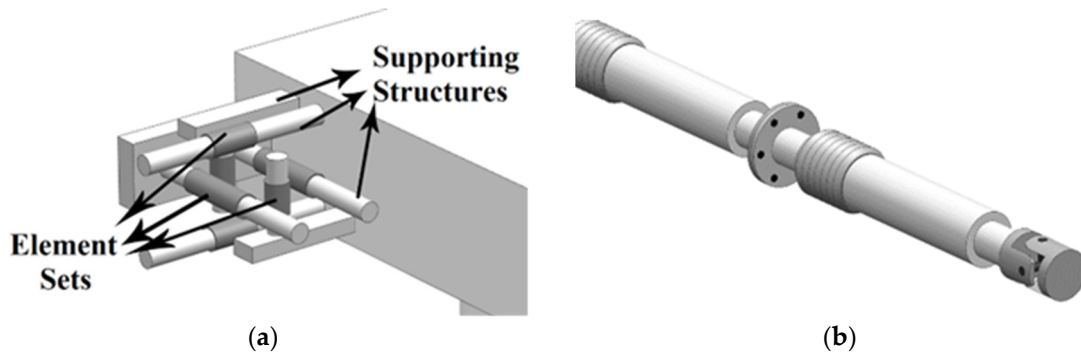


Figure 5. Concept of connection structures: (a) general layout; (b) connection elements.

Under survival conditions, the extreme value of the connection loads  $F_{C-S}$  and relative motions between modules can be calculated with:

$$\begin{cases} F_{C-S} = 3.72 \sqrt{\int_{\omega_{\min}}^{\omega_{\max}} S_S(\omega) \text{diag}(vabs(F_{cc}(\omega))) vabs(F_{cc}(\omega)) d\omega} \\ X_{RE-S} = 3.72 \sqrt{\int_{\omega_{\min}}^{\omega_{\max}} S_S(\omega) \text{diag}(vabs(A_c u(\omega))) vabs(A_c u(\omega)) d\omega} \end{cases} \quad (20)$$

Since there are 72 optimization variables for the modular floating wind farm in the present work, the process of optimization is to search for the optimum in a 72-dimensional space.

For the  $j$ th direction of the  $i$ th connection structure, the element arrangement would satisfy:

$$\begin{cases} N_{para-i-j} k_e / N_{seri-i-j} = k_i \\ N_{seri-i-j} S_e \geq x_{RE-SLS-i-j} \\ N_{para-i-j} B_e \geq f_{C-SLS-i-j} \\ 0.5 \times 10^6 \text{ N/m} \leq k_e \leq 1.5 \times 10^6 \text{ N/m} \end{cases} \quad (21)$$

where,  $(N_{para} N_{seri})$  are the numbers of connection elements in parallel and serial; and  $S_e$ ,  $k_e$ , and  $B_e$  are the stroke, stiffness, and bearing capacity of the connection elements. The minimum integer combination of  $(N_{para} N_{seri})$  satisfying Equation (21) will be the arrangement of the connection element.

To reduce the mathematical complexity, the stiffness of the connection elements is set to a continuous range, the properties of the connection elements are listed in Table 4. The range of stiffness is from  $1 \times 10^6$  N/m to  $1 \times 10^{10}$  N/m, and the range of the damping ratio is from 0 to 1.0.



**Table 4.** Properties of the connection elements.

Property	Unit	Value
Stiffness ( $k_e$ )	N/m	$0.5\text{--}1.5 \times 10^6$
Stroke ( $S_e$ )	m	0.6
Max Load ( $B_e$ )	N	$1.5 \times 10^6$

Additionally, considering the structural feasibility, constraints on the number of connection elements in serial are set as:

$$\begin{cases} N_{seri-x} \leq 5 \\ N_{seri-y} \leq 5 \\ N_{seri-z} \leq 4 \end{cases} \quad (22)$$

When ( $N_{para}$   $N_{seri}$ ) is obtained, the number of connection elements required at the initial stage of the modular floating wind farm  $N_{int}$  can be expressed as:

$$N_{int} = \sum_{i=1}^{24} \sum_{j=x,y,z} N_{seri-i-j} N_{para-i-j} \quad (23)$$

In the phase of operation, the cost of maintenance can be expressed as the number of elements for replacement. In the present work, the working life of the structure is set to be 20 years, and the annual frequency of replacement, set as the element-to-element joint, is 0.02, and the element-to-module joint is 0.04. Therefore, for the whole service life, the expectation of replacement for element-to-element and element-to-module ( $E_{ete}$ ,  $E_{etm}$ ) are:

$$\begin{cases} E_{ete} = 0.40 \\ E_{etm} = 0.80 \end{cases} \quad (24)$$

Then, the total expectation of elements for replacement  $N_{rep}$  can be calculated as:

$$N_{rep} = \sum_{i=1}^{24} \sum_{j=x,y,z} (E_{ete} (N_{seri-i-j} - 1) N_{para-i-j} + 2E_{etm} N_{para-i-j}) \quad (25)$$

Based on the calculations above, the function of economics  $G(\mathbf{R})$ , can be specified as:

$$G(\mathbf{R}) = -(N_{int} + N_{rep}) \quad (26)$$

For the function that characterizes the performance of the structure  $F(\mathbf{X})$ , the operation condition is selected, and the safety factors are taken as the quantity scale. For most types of responses, the number of magnitudes of different modules will not vary to a large extent; therefore, the arithmetic mean values of the safety factor are taken to represent the response magnitude and the vector of safety factors for various types of responses can be expressed as:

$$\left\{ \begin{aligned}
 SF_1 &= \frac{1}{6} \left( 2(\mathbf{X}_{OLS})^T \mathbf{E}_z \left( \sqrt{\int_{\omega_{\min}}^{\omega_{\max}} S_{OLS}(\omega) \text{diag}(vabs(\mathbf{u}(\omega))) vabs(\mathbf{u}(\omega)) d\omega} \right)^{-1} \right) \\
 SF_2 &= \frac{1}{6} \left( 2(\mathbf{X}_{OLS})^T \mathbf{E}_{rx} \left( \sqrt{\int_{\omega_{\min}}^{\omega_{\max}} S_{OLS}(\omega) \text{diag}(vabs(\mathbf{u}(\omega))) vabs(\mathbf{u}(\omega)) d\omega} \right)^{-1} \right) \\
 SF_3 &= \frac{1}{6} \left( 2(\mathbf{X}_{OLS})^T \mathbf{E}_{ry} \left( \sqrt{\int_{\omega_{\min}}^{\omega_{\max}} S_{OLS}(\omega) \text{diag}(vabs(\mathbf{u}(\omega))) vabs(\mathbf{u}(\omega)) d\omega} \right)^{-1} \right) \\
 SF_4 &= \frac{1}{6} \left( 2(\mathbf{X}_{OLS})^T \mathbf{E}_{rz} \left( \sqrt{\int_{\omega_{\min}}^{\omega_{\max}} S_{OLS}(\omega) \text{diag}(vabs(\mathbf{u}(\omega))) vabs(\mathbf{u}(\omega)) d\omega} \right)^{-1} \right) \\
 SF_5 &= \frac{1}{6} \left( 2(\mathbf{V}_{OLS})^T \mathbf{E}_x \left( \sqrt{\int_{\omega_{\min}}^{\omega_{\max}} S_{OLS}(\omega) \text{diag}(vabs(\omega \mathbf{A}_{hub} \mathbf{u}(\omega))) vabs(\omega \mathbf{A}_{hub} \mathbf{u}(\omega)) d\omega} \right)^{-1} \right) \\
 SF_6 &= \frac{1}{6} \left( 2(\mathbf{V}_{OLS})^T \mathbf{E}_y \left( \sqrt{\int_{\omega_{\min}}^{\omega_{\max}} S_{OLS}(\omega) \text{diag}(vabs(\omega \mathbf{A}_{HUB} \mathbf{u}(\omega))) vabs(\omega \mathbf{A}_{HUB} \mathbf{u}(\omega)) d\omega} \right)^{-1} \right) \\
 SF_7 &= \frac{1}{6} \left( 2(\mathbf{a}_{OLS})^T \mathbf{E}_x \left( \sqrt{\int_{\omega_{\min}}^{\omega_{\max}} S_{OLS}(\omega) \text{diag}(vabs(\omega^2 \mathbf{A}_{HUB} \mathbf{u}(\omega))) vabs(\omega^2 \mathbf{A}_{HUB} \mathbf{u}(\omega)) d\omega} \right)^{-1} \right) \\
 SF_8 &= \frac{1}{6} \left( 2(\mathbf{a}_{OLS})^T \mathbf{E}_y \left( \sqrt{\int_{\omega_{\min}}^{\omega_{\max}} S_{OLS}(\omega) \text{diag}(vabs(\omega^2 \mathbf{A}_{HUB} \mathbf{u}(\omega))) vabs(\omega^2 \mathbf{A}_{HUB} \mathbf{u}(\omega)) d\omega} \right)^{-1} \right)_i \\
 SF_9 &= \frac{1}{6} \left( 2(\mathbf{a}_{OLS})^T \mathbf{E}_z \left( \sqrt{\int_{\omega_{\min}}^{\omega_{\max}} S_{OLS}(\omega) \text{diag}(vabs(\omega^2 \mathbf{A}_{HUB} \mathbf{u}(\omega))) vabs(\omega^2 \mathbf{A}_{HUB} \mathbf{u}(\omega)) d\omega} \right)^{-1} \right)
 \end{aligned} \right. \tag{27}$$

where  $E_x E_y E_z E_{rx} E_{ry} E_{rz}$  are the matrices of extraction for various DOFs, and the sign “-1” on the vector denotes constructing a vector whose components are the reciprocals of the input ones.

As the constraints are set independently from the response properties, for different types of responses, the safety factors may vary to a large extent. To give a generalized assessment of the dynamic performance of the connection parameter, the arithmetic mean value or weighted mean value would not be appropriate due to their inability to get rid of components too high in magnitude. Meanwhile, when the safety factor is over 10, it would be excessive, and the ones with lower safety factors are worth more attention. To more accurately characterize the dynamic responses while accenting low components of the safety factors, the function of response properties  $F(\mathbf{X})$  comes in the form of:

$$F(\mathbf{X}) = \frac{9}{\sum_{i=1}^9 SF_i^{-1}} \tag{28}$$

Under this form, a continuous mathematical form is obtained while the effects of the over-high components are lowered.

Therefore, the function of value VA can be expressed as:

$$VA = G(\mathbf{R})/F(\mathbf{X}) = -(N_{int} + N_{rep}) \sum_{i=1}^9 SF_i^{-1} / 9 \tag{29}$$

To give a direct illustration of VA, uniform connection parameter combinations (identical connection stiffness and damping ratio) are taken as representatives, variations in VA with uniform connection parameters are shown in Figure 6.

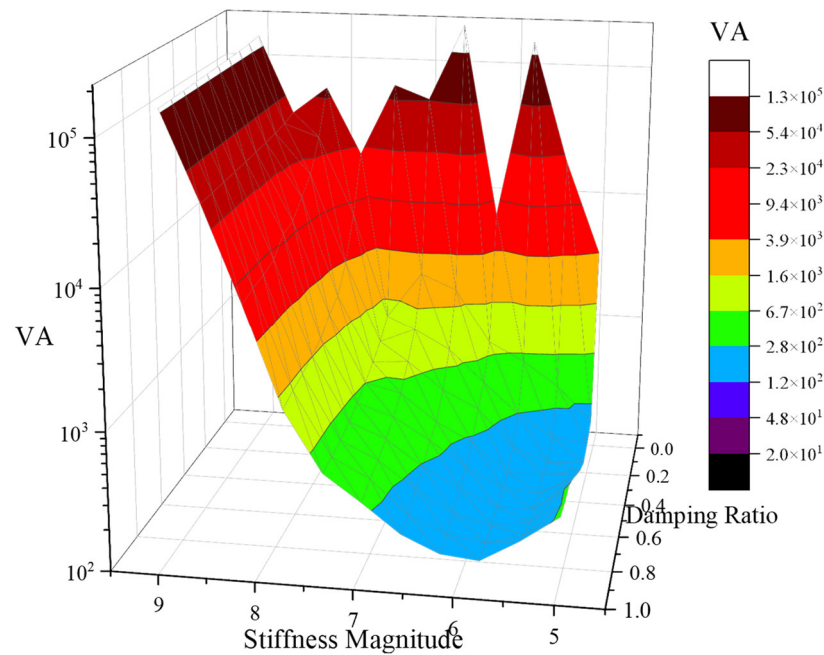


**Figure 6.** Variations in VA under uniform connection parameters.

As can be observed in Figure 6, the magnitude of stiffness dominates the values of VA, and a general tendency of rising with stiffness is quite obvious. For parts of VA, due to the properties of Equation (28), it is quite hard for the function of response properties  $F(X)$  to exceed 10; meanwhile, for the function of economics  $G(R)$ , the value would rise in a linear-like pattern due to Equation (21) under the state of high connection stiffness. Under this condition, optimization of VA under various constraints indicates an engineering issue of spending less on similar response properties or obtaining better response properties with similar costs, i.e., obtaining the balance between costs and response properties in the feasible region constraint by design requirements. In addition, as can be observed from Figure 6, the lowest variation in VA tends to occur around the stiffness magnitude of  $1 \times 10^6$  N/m; however, due to the complexity and strictness in constraints, for the cases from Figure 6 in the stiffness magnitude of  $1 \times 10^6$  N/m, the constraints are not all met, and the lowest uniform stiffness which can meet all constraints is around  $1.58 \times 10^7$  N/m. Therefore, based on the data from the uniform connection parameters, the optimum in the 72-dimensional space will quite likely be a combination whose majority components of stiffness are in the magnitude of  $1 \times 10^6$  N/m while satisfying all constraints.

#### 4. Results and Discussion

Due to the high number of parameters and the complexity of the constraints and target function, the genetic algorithm is selected for the optimization with Equations (16), (17), and (22) as constraints and Equation (29) as the target function. The MATLAB (2017b) GA toolbox is taken as the optimization tool, a population of 1000 is selected, and a function tolerance of  $1 \times 10^{-6}$  is taken as the convergence scale. Due to the complexity of the constraints, the population creation, mutation, and crossover are constraint-dependent. The initial population is auto-generated by constraint-dependent methods, and an elite rate of 0.02 is taken for the optimization process. After about 120 h of calculation, the optimization results are obtained due to a low average change; the process of optimization is shown in Figure 7. As can be learned from Figure 7b, at the time of stopping, the majority of the individuals are around the value of the obtained optimum (177.92) due to the complexity and strictness of the constraints.

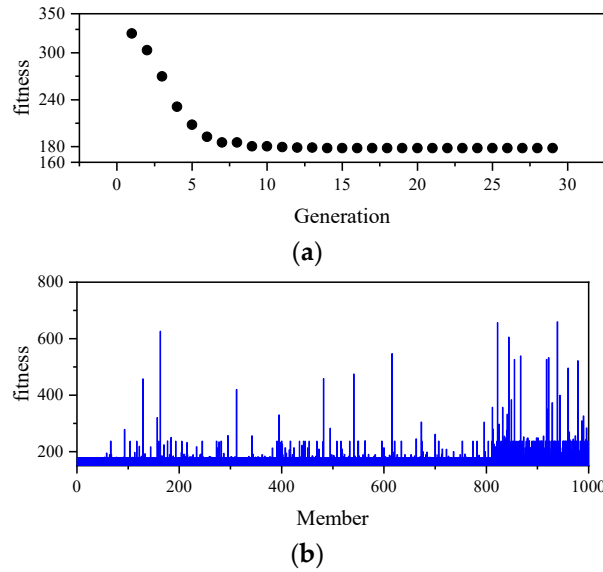


Figure 7. Process of optimization: (a) best fitness for each generation; (b) individuals at stopping.

The result of the optimization is shown in Figure 8. As shown in Figure 8, the stiffness in longitudinal and vertical directions are all in the magnitude of  $1 \times 10^6$  N/m, for the stiffness in the lateral direction, C2, C3, C5, C14, C15 are in the magnitude of  $1 \times 10^7$  N/m with the rest between  $1 \times 10^6$  and  $2.1 \times 10^6$  N/m. In the tri-axial damping ratio, the majority are around 1.0, indicating the positive effects of the damping ratio on the structure responses. From the tendency shown in Figure 6, it is quite evident that lower stiffness tends to be more competitive in the process of optimization; however, due to the strictness of constraints, it is hard for combinations with all stiffness components at the magnitude of  $1 \times 10^6$  N/m to meet the constraints. Therefore, the increase in stiffness for certain connection stiffness components is of great necessity. From the result of optimization, it is quite clear that the increase in lateral stiffness is more beneficial. Contrasting with the constraints in Table 3, the maximum heave response amplitude is 3.79 m, while the constraint is 4 m, i.e., the result of the optimization is quite near the boundary of the feasible region, and the increase in the lateral stiffness works as a method to lower the responses, especially the heave responses, based on the position of the connection structure with higher lateral stiffness. The lowering of the heave response is performed indirectly through lowering the roll and pitch responses of T1.

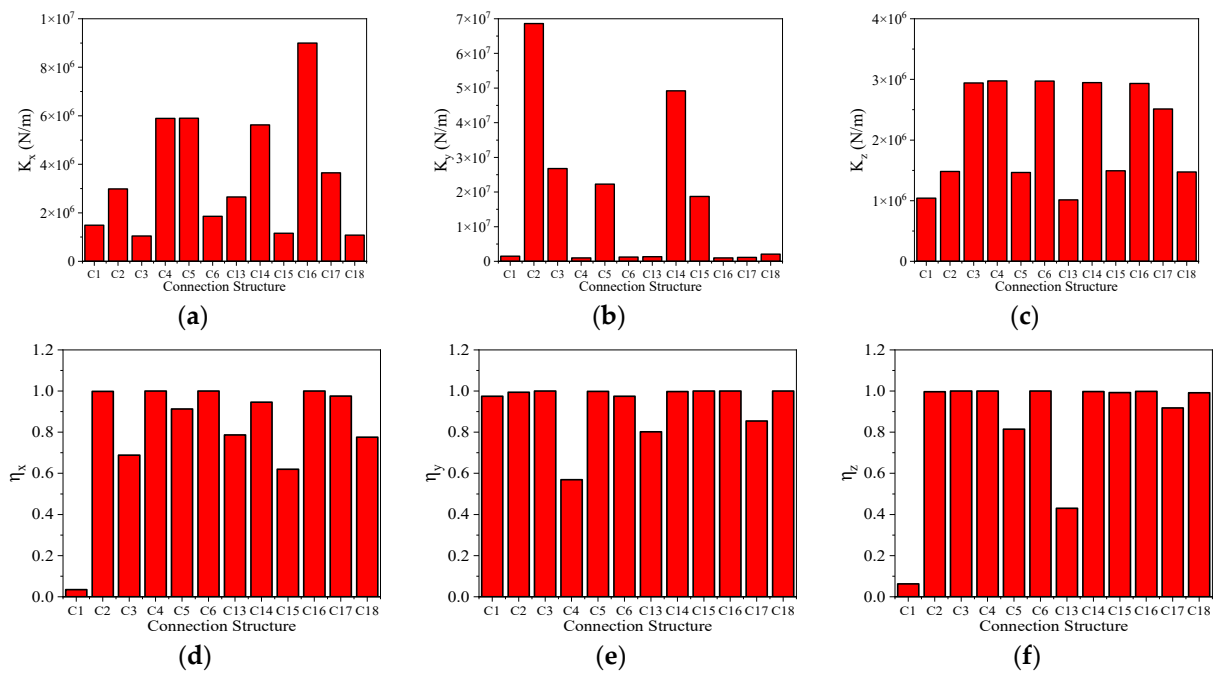
Contrasts between the obtained optimum solution and the uniform connection parameter combination with relatively low stiffness (all tri-axial stiffness set to  $1.58 \times 10^7$  N/m, damping ratio to 1.0,  $VA = 360.58$ ) in responses under operation conditions are listed in Table 5.

Table 5. Contrasts between uniform parameters and optimized parameters in motions.

DOF	Unit	Uniform Parameters				Optimized Parameters			
		COY	T1	T2	T3	COY	T1	T2	T3
Surge	m	0.326	0.338	0.291	0.543	0.263	0.337	0.379	0.62
Sway	m	≈0	0.110	0.203	0.425	≈0	0.123	0.22	0.365
Heave	m	1.423	1.042	0.995	2.146	1.277	0.978	0.898	2.036
Roll	°	≈0	0.266	0.409	0.513	≈0	0.236	0.463	0.571
Pitch	°	0.313	0.331	0.408	0.494	0.419	0.368	0.448	0.533
Yaw	°	≈0	0.104	0.136	0.325	≈0	0.096	0.172	0.44

As listed in Table 5, it is obvious that the relatively high stiffness magnitude in the uniform case does not bring about evident enhancements in motion properties; meanwhile, in the DOFs of sway and heave, the response amplitude under the optimized connection

parameters tends to be lower. As the majority of tri-axial stiffness in the optimized results are in the magnitude of  $1 \times 10^6$  N/m, it is evident that the optimization method in the present work is able to lower connection parameters, while obtaining better responses.



**Figure 8.** Results of the optimization: (a) longitudinal stiffness; (b) transverse stiffness; (c) vertical stiffness; (d) longitudinal damping; (e) transverse damping; (f) vertical damping.

When the optimized connection parameter combination is obtained, the time domain analysis is carried out with ANSYS AQWA (v17.1), and the connection loads are numerically calculated with Equation (9) to Equation (13) by the user-defined subroutine user\_force.

The time domain motion responses under heading waves are displayed in Figure 9. As can be observed from Figure 9, the motion amplitude in surge tends to be slightly higher over the data in Table 5 (the standard deviation in T3 surge from Figure 9a is about 1.5 m); meanwhile, for the rest of the DOFs, the response amplitudes tend to be in good accordance with the results from Table 5. Due to the mooring system and low-frequency wave loads, mean values can be observed in motions, especially in the DOF of surge.

To give a straightforward illustration of the response properties of module motions, the FFT results of the motions of T3 from Figure 9 and the frequency domain analysis (FDA for short) results from Equation (8) ( $\Delta\omega = 0.02$  rad/s) are put in contrast in Figure 10. As can be observed from Figure 10, the FFT results are mainly in the region of wave frequency except for the DOF of yaw, where significant low-frequency components are observed. Contrasting the yaw response in Figure 9f and the FFT results in Figure 10f, it is obvious that the low-frequency motions in the DOF of yaw are the result of the rigid body motion of the whole structure as indicated by the yaw motions of the COY module, and the higher surge responses may also be attributed to the low-frequency yaw responses. Contrasting the tendencies from the FFT and the frequency domain analysis, good accordance between the two analytical approaches can be obtained, as the time domain analysis approach and the frequency domain analysis approach are irrelevant, and the effectiveness of the analytical approaches can be validated.

For the connection loads, the contrast between FFT results from the time domain loads and frequency domain analysis results from Equation (8) are displayed in Figure 11, C2, C4, and C15 are taken as representative.



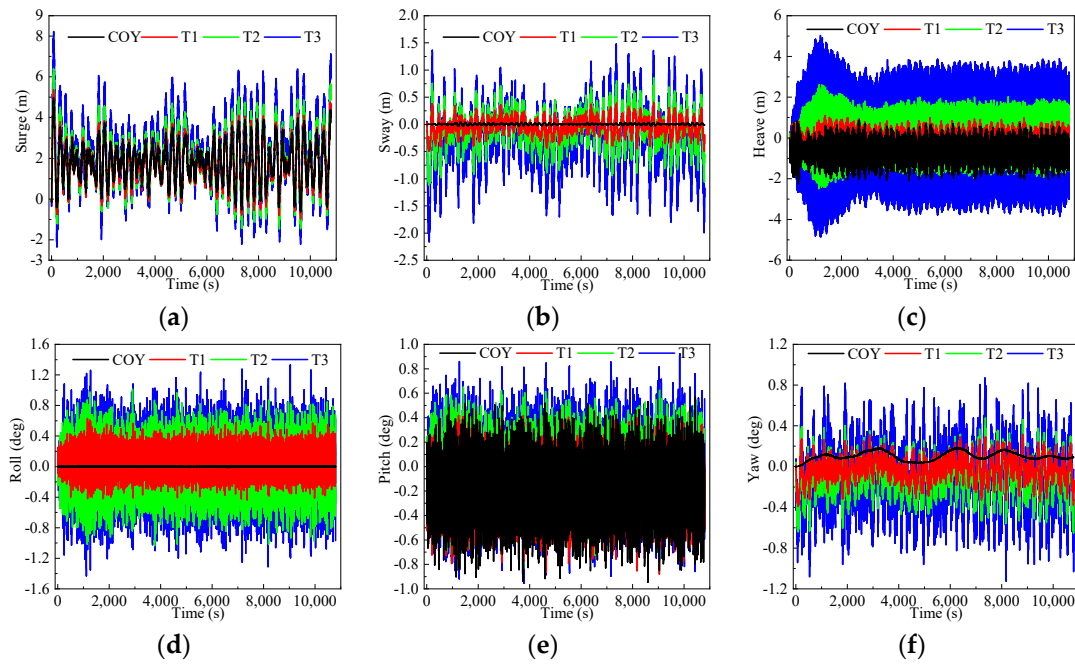


**Figure 9.** Time domain motions of the modules: (a) surge; (b) sway; (c) heave; (d) roll; (e) pitch; (f) yaw.

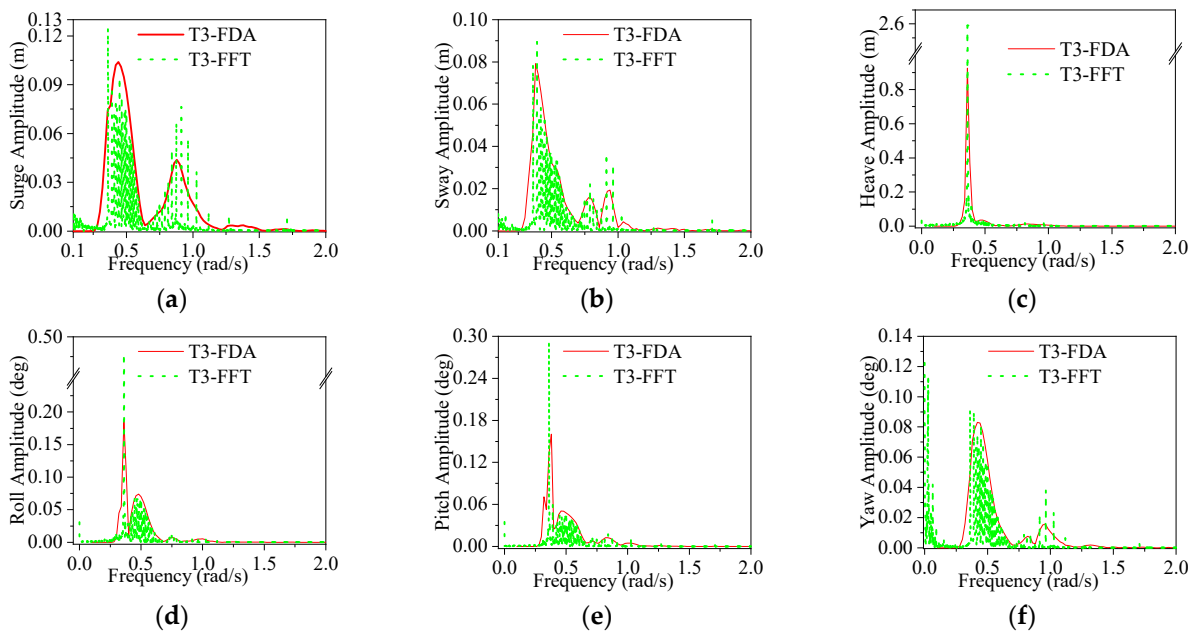


**Figure 10.** Frequency domain properties of the motions of T3: (a) Surge; (b) Sway; (c) Heave; (d) Roll; (e) Pitch; (f) Yaw.

As can be observed from Figure 11, wave frequency components take up the major parts, and the low-frequency part is mainly at  $\omega = 0$ , i.e., the mean load induced by the mooring system and mean wave drift loads. For the wave frequency region, as it is clear from Figure 11, good accordance can be observed between the time domain approach and frequency domain approach, indicating the effectiveness of the analysis and the basis of optimization.

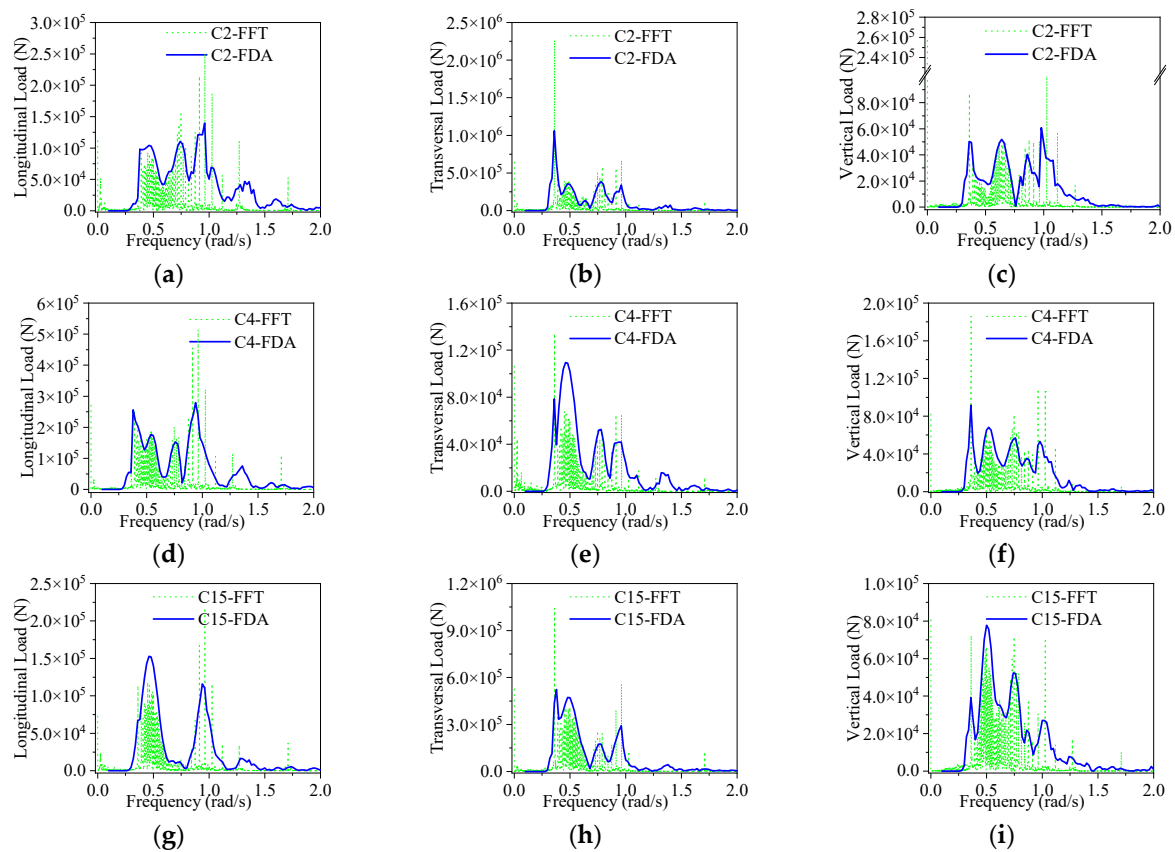


**Figure 11.** Frequency domain properties of tri-axial connection loads on connection structure: (a–c): C2; (d–f): C4; (g–i) C15.

### 5. Conclusions

In the present work, a quantified methodology to assess the connection parameter for a novel type of modular floating wind farm is proposed based on the frequency domain analysis, and optimization is carried out to obtain the optimum connection parameter. A time domain approach for the calculation of connection loads for modular floating structures with weather-vane ability is proposed and put into contrast with the frequency domain analysis.

From the FFT results of the time domain results, the wave frequency domain takes up the most part of both motion responses and connection loads; based on this fact, the optimization based on the frequency domain analysis approach is reasonable.

In the wave frequency region, good accordance between the time domain approach and frequency domain approach is obtained, as the two approaches are irrelevant, and the effectiveness of the analysis methods can be verified.

From the optimized connection parameters, it can be found that the most appropriate tri-axial stiffness according to present studies is in the magnitude from  $1 \times 10^6$  to  $7 \times 10^7$  N/m, and the damping ratio is close to 1.0 for most connection structures.

From the comparisons with uniform connection parameters, it is evident that the optimization methodology in the present work is able to reduce connection parameters while enhancing the general performance of the structures.

In the early phase of this preliminary study, the methodology in the present work offers an approach that is generally suitable for more precise future analyses, thus enhancing the efficiency in design and analysis.

**Author Contributions:** Conceptualization, Y.Z.; writing—original draft preparation, Y.Z.; project administration, D.L.; supervision, H.L. All authors have read and agreed to the published version of the manuscript.

**Funding:** This research received no external funding.

**Data Availability Statement:** The original contributions presented in the study are included in the article, further inquiries can be directed to the corresponding author.

**Conflicts of Interest:** Author Yuming Zhang and Da Li was employed by the company CNOOC Research Institute Ltd. The remaining authors declare that the research was conducted in the absence of any commercial or financial relationships that could be construed as a potential conflict of interest.

## References

1. Stehly, T.; Beiter, P.; Duffy, P. *2019 Cost of Wind Energy Review*; National Renewable Energy Lab. (NREL): Golden, CO, USA, 2020.
2. Wang, C.M.; Utsunomiya, T.; Wee, S.C.; Choo, Y.S. Research on Floating Wind Turbines: A Literature Survey. *IES J. Part A Civ. Struct. Eng.* **2010**, *3*, 267–277. [[CrossRef](#)]
3. Gelotte, L.; Nilsson, A.L. *Optimal Placement of Floating Two-Turbine Foundations in Offshore Wind Farms*; KTH Royal Institute of Technology: Stockholm, Sweden, 2017.
4. Avanessova, N.; Land, J.; Lee, A.; Lazakis, I.; Thomson, C. Comparison of Operation and Maintenance of Floating 14 MW Turbines and Twin 10 MW Turbines. *ASME Open J. Eng.* **2023**, *2*, 021031. [[CrossRef](#)]
5. Manabe, H.; Uehiro, T.; Utiyama, M.; Esaki, H.; Kinoshita, T.; Takagi, K.; Okamura, H.; Satou, M. Development of the Floating Structure for the Sailing-Type Offshore Wind Farm. In Proceedings of the OCEANS 2008-MTS/IEEE Kobe Techno-Ocean, Kobe, Japan, 8–11 April 2008; IEEE: Piscataway, NJ, USA, 2008; pp. 1–4.
6. Zhang, Y.; Liu, H. A Novel Structural Configuration of Modular Floating Wind Farms with Self-Adaptive Property. *J. Offshore Mech. Arct. Eng.* **2021**, *143*, 052002. [[CrossRef](#)]
7. Lamas-Pardo, M.; Iglesias, G.; Carral, L. A Review of Very Large Floating Structures (VLFS) for Coastal and Offshore Uses. *Ocean Eng.* **2015**, *109*, 677–690. [[CrossRef](#)]
8. Newman, J.N. Wave Effects on Deformable Bodies. *Appl. Ocean Res.* **1994**, *16*, 47–59. [[CrossRef](#)]
9. Newman, J.N. Wave Effects on Multiple Bodies. *Hydrodyn. Ship Ocean. Eng.* **2001**, *3*, 3–26.
10. Palo, P. Mobile Offshore Base: Hydrodynamic Advancements and Remaining Challenges. *Mar. Struct.* **2005**, *18*, 133–147. [[CrossRef](#)]
11. Mcallister, K.R. Mobile Offshore Bases—An Overview of Recent Research. *Mar. Sci. Technol.* **1997**, *2*, 173–181. [[CrossRef](#)]
12. Zheng, S.; Zhang, Y.H.; Zhang, Y.; Sheng, W. Numerical Study on the Dynamics of a Two-Raft Wave Energy Conversion Device. *J. Fluids Struct.* **2015**, *58*, 271–290. [[CrossRef](#)]
13. Henderson, R. Design, Simulation, and Testing of a Novel Hydraulic Power Take-off System for the Pelamis Wave Energy Converter. *Renew. Energy* **2006**, *31*, 271–283. [[CrossRef](#)]
14. Michailides, C.; Angelides, D.C. Modeling of Energy Extraction and Behavior of a Flexible Floating Breakwater. *Appl. Ocean Res.* **2012**, *35*, 77–94. [[CrossRef](#)]
15. Riggs, H.R.; Ertekin, R.C.; Mills, T.R.J. Characteristics of the Wave Response of Mobile Offshore Bases. In Proceedings of the 18th International Conference on Offshore Mechanics and Arctic Engineering, St. John's, NL, Canada, 11–16 July 1999; pp. 1–9.
16. Riggs, H.R.; Ertekin, R.C.; Mills, T.R.J. Comparative Study of RMFC and FEA Models for the Wave-Induced Response of a MOB. *Mar. Struct.* **2000**, *13*, 217–232. [[CrossRef](#)]
17. Zhang, Y.; Liu, H. Methodology for the Assessment and Optimization of Connection Parameter Combinations for Modular Floating Structures. *J. Offshore Mech. Arct. Eng.* **2020**, *143*, 021301. [[CrossRef](#)]
18. Liang, Z.; Liu, H. Layout Optimization of an Offshore Floating Wind Farm Deployed with Novel Multi-Turbine Platforms with the Self-Adaptive Property. *Ocean Eng.* **2023**, *283*, 115098. [[CrossRef](#)]
19. Liang, Z.; Liu, H. Layout Optimization of a Modular Floating Wind Farm Based on the Full-Field Wake Model. *Energies* **2022**, *15*, 809. [[CrossRef](#)]
20. Robertson, A.; Jonkman, J.; Masciola, M.; Song, H.; Goupee, A.; Coulling, A.; Luan, C. *Definition of the Semisubmersible Floating System for Phase II of OC4*; National Renewable Energy Lab. (NREL): Golden, CO, USA, 2014.
21. Jonkman, J.; Butterfield, S.; Musial, W.; Scott, G. *Definition of a 5-MW Reference Wind Turbine for Offshore System Development*; National Renewable Energy Lab. (NREL): Golden, CO, USA, 2009.
22. ANSYS Inc. *AQWA Theory Manual*; ANSYS Inc.: Canonsburg, PA, USA, 2016; Volume 15317.
23. Zhang, Y.; Liu, H. Impact of Connection Properties on Dynamic Response of Modular Floating Structures. In Proceedings of the ASME 2018 37th International Conference on Ocean, Offshore and Arctic Engineering, Madrid, Spain, 17–22 June 2018; American Society of Mechanical Engineers: New York, NY, USA, 2018; pp. 1–11.
24. Faltinsen, O.M. *Sea Loads on Ships and Ocean Structures*; Cambridge University: Cambridge, UK, 1990.

**Disclaimer/Publisher's Note:** The statements, opinions and data contained in all publications are solely those of the individual author(s) and contributor(s) and not of MDPI and/or the editor(s). MDPI and/or the editor(s) disclaim responsibility for any injury to people or property resulting from any ideas, methods, instructions or products referred to in the content.